Photoinduced Electron Transfer in Covalently Linked Ruthenium Tris(bipyridyl)-Viologen Molecules: Observation of Back Electron Transfer in the Marcus Inverted Region

Edward H. Yonemoto,[†] Richard L. Riley,[†] Yeong Il Kim,[†] Stephen J. Atherton,[‡] Russell H. Schmehl,*[,§] and Thomas E. Mallouk*[,†]

Contribution from the Department of Chemistry and Biochemistry and Center for Fast Kinetics Research, University of Texas at Austin, Austin, Texas 78712, and Department of Chemistry, Tulane University, New Orleans, Louisiana 70118. *Received February 3, 1992*

Abstract: The rates of photoinduced electron transfer (ET) in a series of donor-acceptor molecules (4,4′-R_2-2,2′-bipyridine)$_2$Ru(1-(4-CH_3-2,2′-bipyridine-4′-yl-$(CH_2)_n$)-4,4′-bipyridinediium-1′-R′)$^{4+}$ (R = H, CH_3; R′ = CH_3, CH_2CN; n = 1, 2) were studied by picosecond flash photolysis/transient absorbance techniques. The rate of intramolecular forward ET (MLCT quenching) in acetonitrile varied with $-\Delta G°$ according to classical Marcus theory for n = 2, but not for n = 1. The back ET reactions for both n = 1 and n = 2 showed an inverted rate behavior described quantitatively by semiclassical Marcus theory. For the n = 2 compounds, the value of $|V(r)|^2$ ($V(r)$ ≡ electron-exchange matrix element) was approximately 1 order of magnitude higher for the forward than for the back ET reactions. This difference was rationalized in terms of a larger distance over which the back reaction (viologen-to-metal) occurs relative to the forward reaction (bipyridine-to-viologen). Cage-escape efficiencies for a series of Ru(bpy)$_3^{2+}$ electron donors and viologen acceptors did not show any apparent relationship to driving force for the back ET reaction. In this case, geometric factors are more important than energetic factors in controlling the rates of back reaction and cage escape.

Electron-transfer reactions play a key role in chemistry and biology, and understanding the factors which control their rates is of obvious practical importance.[1] In both natural and artificial photosynthetic systems, the competition between productive forward- and energy-wasting reverse-electron-transfer rates determines the quantum yield for light-to-chemical energy conversion. In the bacterial photosynthetic reaction center,[2] for example, the quantum efficiency is essentially unity because, at each step in the electron-transport chain, the rate of the forward transfer exceeds that of charge recombination by 2 orders of magnitude or more.[3] It is now well established that Nature makes profitable use of the Marcus inverted region,[4] i.e., the slowing down of electron-transfer rates with increasing reaction exothermicity at large values of $-\Delta G°_{el}$, in order to retard charge recombination at the first branch point (bacteriopheophytin) in this chain.

In synthetic systems, the existence of the Marcus inverted electron-transfer region has been verified experimentally several times. Most of these systems consist of organic molecules, examined in solvents of relatively low polarity and reorganization energy, as covalently linked donor-acceptor diads,[5] geminate radical ion pairs,[6] and neutral radicals formed by photolysis of ion pairs.[7] There are also examples of inverted-region electron-transfer behavior in inorganic systems.[8] Two of these involve ligand-ligand charge recombination in (2,2′-bipyridine)Re^I-$(CO)_3$L, where L is a phenothiazene[8a] or dimethylaniline[8b] electron donor, and a third involves ligand-metal electron transfer in dimeric iridium(I)-alkylpyridinium complexes.[8c]

Among inorganic photosensitizers which are promising for artificial photosynthetic systems, ruthenium tris(2,2′-bipyridyl) (Ru(bpy)$_3^{2+}$) and its derivatives have been most widely studied.[9] These molecules possess endearing qualities, such as photostability in water, high extinction coefficients in the visible region, and relatively long-lived excited states, the combination of which is sufficiently rare that few good alternatives exist. Since the excess free energy of the excited metal-to-ligand charge-transfer (MLCT) state is about 2.1 eV in these molecules, it is reasonable to expect that back electron transfer between them and either donor or acceptor quenchers of appropriate redox potential might occur in the inverted region, in solvents of moderate polarity. If this is so, then maximizing the free energy change for the back reaction should help to improve the quantum efficiency for productive electron transfer in artificial photosynthetic systems which incorporate Ru(bpy)$_3^{2+}$ and its derivatives.

In this paper, we show that back electron transfer between covalently linked viologen electron acceptors and ruthenium tris(bipyridyl) does in fact occur in the inverted rate region and that both the forward and back electron transfers are described quantitatively by semiclassical Marcus theory. We note also that this behavior, in a system involving reduced acceptor-to-metal electron transfer, is consistent with previous observations of an energy gap law dependence of excited-state lifetimes, wherein

[†] Department of Chemistry and Biochemistry, University of Texas at Austin.
[‡] Center for Fast Kinetics Research, University of Texas at Austin.
[§] Tulane University.

(1) (a) Miller, J. R. *New J. Chem.* **1987**, *11*, 83. (b) Bowler, B. E.; Raphael, A. L.; Gray, H. B. *Prog. Inorg. Chem.* **1990**, *38*, 259.
(2) (a) Deisenhofer, J.; Epp, O.; Miki, K.; Huber, R.; Michel, H. *J. Mol. Biol.* **1984**, *180*, 385. (b) Deisenhofer, J.; Epp, O.; Miki, K.; Huber, R.; Michel, H. *Nature* **1985**, *318*, 618. (c) Allen, P.; Feher, G.; Yeates, T. O.; Rees, D. C.; Deisenhofer, J.; Michel, H.; Huber, R. *Proc. Natl. Acad. Sci. U.S.A.* **1986**, *83*, 8589. (d) Chang, C. H.; Tiede, D.; Tang, J.; Smith, U.; Norris, J.; Schiffer, M. *FEBS Lett.* **1986**, *205*, 82.
(3) (a) Boxer, S. G. *Biochim. Biophys. Acta* **1983**, 726, 265. (b) Martin, J. L.; Breton, J.; Hoff, A. J.; Migus, A.; Antonetti, A. *Proc. Natl. Acad. Sci. U.S.A.* **1986**, *83*, 957. (c) Breton, J.; Martin, J. L.; Migus, A.; Antonetti, A.; Orszag, A. *Proc. Natl. Acad. Sci. U.S.A.* **1986**, *83*, 5121. (d) Kaufman, K. J.; Dutton, P. L.; Netzel, T. L.; Leigh, J. S.; Rentzepis, P. M. *Science* **1975**, *188*, 1301. (e) Gunner, M. R.; Robertson, D. E.; Dutton, P. L. *J. Phys. Chem.* **1986**, *90*, 3783.
(4) (a) Marcus, R. A. *J. Chem. Phys.* **1956**, *24*, 966. (b) Marcus, R. A. *Discuss. Faraday Soc.* **1960**, *29*, 21. (c) Marcus, R. A. *Annu. Rev. Phys. Chem.* **1964**, *15*, 155.
(5) (a) Calcaterra, L. T.; Closs, G. L.; Miller, J. R. *J. Am. Chem. Soc.* **1983**, *105*, 670. (b) Closs, G. L.; Miller, J. R. *Science* **1988**, *240*, 440 and references therein. (c) Liang, N.; Miller, J. R.; Closs, G. L. *J. Am. Chem. Soc.* **1990**, *112*, 5353. (d) Wasielewski, M. R.; Niemczyk, M. P.; Svec, W. A.; Pewitt, E. B. *J. Am. Chem. Soc.* **1985**, *107*, 1080.
(6) (a) Ohno, T.; Yoshimura, A.; Shioyama, H.; Mataga, N. *J. Phys. Chem.* **1987**, *91*, 4365. (b) Gould, I. R.; Ege, D.; Mattes, S. L.; Farid, S. *J. Am. Chem. Soc.* **1987**, *109*, 3794. (c) Gould, I. R.; Moody, R.; Farid, S. *J. Am. Chem. Soc.* **1988**, *110*, 7242. (d) Gould, I. R.; Farid, S. *J. Am. Chem. Soc.* **1988**, *110*, 7883. (e) Mataga, N.; Kanda, Y.; Asahi, T.; Miyasaka, H.; Okada, T.; Kakitani, T. *Chem. Phys.* **1988**, *127*, 239. (f) Gould, I. R.; Moser, J. E.; Armitage, B.; Farid, S.; Goodman, J. L.; Herman, M. S. *J. Am. Chem. Soc.* **1989**, *111*, 1917.
(7) Zou, C.; Miers, J. B.; Ballew, R. M.; Dlott, D. D.; Schuster, G. B. *J. Am. Chem. Soc.* **1991**, *113*, 7823.
(8) (a) Chen, P.; Duesing, R.; Tapolsky, G.; Meyer, T. J. *J. Am. Chem. Soc.* **1989**, *111*, 1917. (b) MacQueen, D. B.; Schanze, K. S. *J. Am. Chem. Soc.* **1991**, *113*, 7470. (c) Fox, L. S.; Kozik, M.; Winkler, J. R.; Gray, H. B. *Science* **1990**, *247*, 1069.
(9) (a) Meyer, T. J. *Acc. Chem. Res.* **1989**, *22*, 163. (b) Kalyanasundaram, K. *Coord. Chem. Rev.* **1982**, *46*, 159.

0002-7863/92/1514-8081$03.00/0

nonradiative decay of the excited state involves ligand-to-metal electron transfer.[8a,9a]

Experimental Section

Materials. Tetrahydrofuran used in the synthesis of 4-(2-methoxyethyl)-4'-methyl-2,2'-bipyridine was HPLC grade and was opened immediately prior to use. The acetonitrile used in the syntheses was distilled from boron oxide under nitrogen. The 4,4'-dimethyl-2,2'-bipyridine was a gift from Prof. C. Michael Elliott and was recrystallized from ethyl acetate. All other materials were of reagent grade quality and used as received from commercial sources. CHN elemental analyses were carried out by Atlantic Microlabs, Inc., Northcross, GA.

[Ru(2,2'-bipyridine)$_2$(4-(bromomethyl)-4'-methyl-2,2'-bipyridine)](PF$_6$)$_2$ and [Ru(4,4'-dimethyl-2,2'-bipyridine)$_2$(4-(bromomethyl)-4'-methyl-2,2'-bipyridine)](PF$_6$)$_2$. [Ru(2,2'-bipyridine)$_2$(4-(bromomethyl)-4'-methyl-2,2'-bipyridine)](PF$_6$)$_2$ was synthesized according to a literature method.[10] [Ru(4,4'-dimethyl-2,2'-bipyridine)$_2$(4-(bromomethyl)-4'-methyl-2,2'-bipyridine)](PF$_6$)$_2$ was prepared similarly using Ru(4,4'-dimethyl-2,2'-bipyridine)$_2$Cl$_2$·2H$_2$O instead of Ru(2,2'-bipyridine)$_2$Cl$_2$·2H$_2$O.[11] However, [Ru(4,4'-dimethyl-2,2'-bipyridine)$_2$-(4-(hydroxymethyl)-4'-methyl-2,2'-bipyridine)](PF$_6$)$_2$ when chromatographed on silica gel with a 5:4:1 mixture of acetonitrile/water/saturated potassium nitrate separated into three bands. The second band, which was luminescent, contained the product; the first band was brownish-black and nonluminescent. Excess KNO$_3$ was removed from the product by evaporating the solvent under reduced pressure to give a red slurry of KNO$_3$ crystals and then adding acetone to precipitate the KNO$_3$ completely. A small amount of ethanol was added to help solvate the product. The solvent was removed under reduced pressure, leaving the product as the nitrate salt, which was then dissolved in water and precipitated with a concentrated solution of ammonium hexafluorophosphate. The hexafluorophosphate salt was then vacuum-filtered and washed with water and then ether. [Ru(4,4'-dimethyl-2,2'-bipyridine)$_2$(4-(hydroxymethyl)-4'-methyl-2,2'-bipyridine)](PF$_6$)$_2$ was converted to [Ru(4,4'-dimethyl-2,2'-bipyridine)$_2$(4-(bromomethyl)-4'-methyl-2,2'-bipyridine)](PF$_6$)$_2$ by the method of Geren et al.[10] ^{1}H NMR (CD$_3$CN) δ: CH$_3$ 2.6, CH$_2$Br 4.7, aromatic 7.3–8.7.

[1-Methyl-4,4'-bipyridinium]PF$_6$. 4,4'-Bipyridine was stirred with a slight excess (1.5 equiv) of iodomethane in methylene chloride at room temperature for 12 h. The yellow precipitate that formed was vacuum-filtered and washed with a small amount of methylene chloride followed by ether. The hexafluorophosphate salt was prepared by dissolving the iodide in water and precipitated with a concentrated solution of ammonium hexafluorophosphate. ^{1}H NMR (CD$_3$CN) δ: CH$_3$ 4.4; aromatic 7.8 (doublet), 8.4 (doublet), 8.8 (doublet of doublets).

[1-(Cyanomethyl)-4,4'-bipyridinium](PF$_6$). 4,4'-Bipyridine was refluxed with a slight excess (1.5 equiv) of bromoacetonitrile in acetonitrile for 12 h. The product precipitated as a brown-green solid, which was vacuum-filtered and washed with ether. The solid was then dissolved in water and precipitated with ammonium hexafluorophosphate. The hexafluorophosphate salt was vacuum-filtered and washed with ether. ^{1}H NMR (CD$_3$CN) δ: CH$_2$CN 6.2; aromatic 8.0 (doublet), 8.9 (doublet of doublets), 9.5 (doublet).

[Ru(2,2'-bipyridine)$_2$(4-((1'-methyl-4,4'-bipyridinediium-1-yl)-methyl)-4'-methyl-2,2'-bipyridine)](PF$_6$)$_4$·2H$_2$O (H1M) and [Ru(4,4'-dimethyl-2,2'-bipyridine)$_2$(4-((1'-methyl-4,4'-bipyridinediium-1-yl)-methyl)-4'-methyl-2,2'-bipyridine)](PF$_6$)$_4$·2H$_2$O (M1M). [Ru(2,2'-bipyridine)$_2$(4-(bromomethyl)-4'-methyl-2,2'-bipyridine)](PF$_6$)$_2$ (0.2 g, 2.1 × 10^{-4} mol) and [Ru(4,4'-dimethyl-2,2'-bipyridine)$_2$(4-(bromomethyl)-4'-methyl-2,2'-bipyridine)](PF$_6$)$_2$ (0.2 g, 2.0 × 10^{-4} mol) were refluxed with a 2-fold excess of [1-methyl-4,4'-bipyridinium]PF$_6$ in 40 mL of dry acetonitrile for 12 h under nitrogen. The acetonitrile was removed under reduced pressure, and the product was then eluted from a silica column using 5:4:1 CH$_3$CN/H$_2$O/saturated aqueous KNO$_3$. The KNO$_3$ was removed by the method described above. The product was dissolved in water, precipitated with ammonium hexafluorophosphate, and washed with water, chloroform, and then ether. [Ru(2,2'-bipyridine)$_2$(4-((1'-methyl-4,4'-bipyridinediium-1-yl)methyl)-4'-methyl-2,2'-bipyridine)](PF$_6$)$_4$·2H$_2$O yield: 0.05 g, 3.7 × 10^{-5} mol (18%). ^{1}H NMR (CD$_3$CN) δ: CH$_3$ 2.5, CH$_3$N$^+$ 4.4, CH$_2$ 6.0, aromatic 7.3–9.6. Anal. Calcd (found): C, 37.32 (36.79); H, 3.06 (2.90); N, 8.10 (8.00). [Ru(4,4'-dimethyl-2,2'-bipyridine)$_2$(4-((1'-methyl-4,4'-bipyridinediium-1-yl)methyl)-4'-methyl-2,2'-bipyridine)](PF$_6$)$_4$·2H$_2$O yield: 0.044 g, 3.1 × 10^{-5} mol (16%). ^{1}H NMR (CD$_3$CN) δ: CH$_3$ 2.6, CH$_3$N$^+$ 4.4, CH$_2$ 6.0, aromatic 7.3–9.6. Anal. Calcd (found): C, 39.21 (38.88); H, 3.50 (3.36); N, 7.78 (7.76).

[Ru(2,2'-bipyridine)$_2$(4-((1'-(cyanomethyl)-4,4'-bipyridinediium-1-yl)methyl)-4'-methyl-2,2'-bipyridine)](PF$_6$)$_4$·2H$_2$O (H1C) and [Ru(4,4'-dimethyl-2,2'-bipyridine)$_2$(4-((1'-(cyanomethyl)-4,4'-bipyridinediium-1-yl)methyl)-4'-methyl-2,2'-bipyridine)](PF$_6$)$_4$·2H$_2$O (M1C). [Ru(2,2'-bipyridine)$_2$(4-(bromomethyl)-4'-methyl-2,2'-bipyridine)](PF$_6$)$_2$ (0.2 g, 2.1 × 10^{-4} mol) and [Ru(4,4'-dimethyl-2,2'-bipyridine)$_2$(4-(bromomethyl)-4'-methyl-2,2'-bipyridine)](PF$_6$)$_2$ (0.16 g, 1.6 × 10^{-4} mol) were refluxed with a 2-fold excess of [1-(cyanomethyl)-4,4'-bipyridinium]PF$_6$ in 40 mL of dry acetonitrile for 12 h under nitrogen. The products were then purified the same way as Ru(2,2'-bipyridine)$_2$(4-((1'-methyl-4,4'-bipyridinediium-1-yl)methyl)-4'-methyl-2,2'-bipyridine)](PF$_6$)$_4$ and [Ru(4,4'-dimethyl-2,2'-bipyridine)$_2$(4-((1'-methyl-4,4'-bipyridinediium-1-yl)methyl)-4'-methyl-2,2'-bipyridine)](PF$_6$)$_4$. The cyanomethyl derivatives are unstable in even slightly alkaline solutions. [Ru(2,2'-bipyridine)$_2$(4-((1'-(cyanomethyl)-4,4'-bipyridinediium-1-yl)methyl)-4'-methyl-2,2'-bipyridine)](PF$_6$)$_4$·2H$_2$O yield: 0.04 g, 2.9 × 10^{-5} mol (14%). ^{1}H NMR (CD$_3$CN) δ: CH$_3$ 2.6, CH$_2$CN 5.8, CH$_2$ 6.0, aromatic 7.3–9.5. Anal. Calcd (found): C, 37.51 (37.30); H, 2.93 (2.80); N, 8.95 (8.91). [Ru(4,4'-dimethyl-2,2'-bipyridine)$_2$(4-((1'-(cyanomethyl)-4,4'-bipyridinediium-1-yl)methyl)-4'-methyl-2,2'-bipyridine)](PF$_6$)$_4$·2H$_2$O yield: 0.028 g, 2.0 × 10^{-5} mol (12%). ^{1}H NMR (CD$_3$CN) δ: CH$_3$ 2.6, CH$_2$CN 5.8, CH$_2$ 6.0, aromatic 7.3–9.3. Anal. Calcd (found): C, 39.36 (39.53); H, 3.37 (3.35); N, 8.61 (8.58).

4-(2-Bromoethyl)-4'-methyl-2,2'-bipyridine. 4-(2-Methoxyethyl)-4'-methyl-2,2'-bipyridine was synthesized by a literature method.[12] 4-(2-Methoxyethyl)-4'-methyl-2,2'-bipyridine (0.35 g, 0.0015 mol) was refluxed for 30 h in 7.0 mL of HBr/acetic acid (45% w/v) and cooled to room temperature. The solution solidified as it cooled, and ice water was added to dissolve the solid. A saturated sodium bicarbonate solution was added slowly to the solution until it ceased to produce carbon dioxide. The solution was then extracted with ether (4 × 50 mL), the extracts were dried over magnesium sulfate and filtered, and the solvent was evaporated at room temperature, yielding a yellow-brown oil. The oil was dissolved in a minimum amount of ether and chromatographed on a short silica column; elution with ether removed the brown impurity. The ether was removed by rotary evaporation at room temperature, leaving a yellow oil as the product (4-(2-bromoethyl)-4'-methyl-2,2'-bipyridine yield: 0.39 g, 0.0014 mol (91%). ^{1}H NMR (CDCl$_3$) δ: CH$_3$ 2.5; CH$_2$ 3.5; CH$_2$Br 3.9; aromatic 7.3, 8.4 (doublet), 8.8 (doublet).

[1-(2-(4'-Methyl-2,2'-bipyridin-4-yl)ethyl)-1'-methyl-4,4'-bipyrinediium](PF$_6$)$_2$. 4-(2-Bromoethyl)-4'-methyl-2,2'-bipyridine (0.3 g, 0.001 mol) and a 2-fold excess of [1-methyl-4,4'-bipyridinium]I were refluxed in 100 mL of acetonitrile for 3 days under nitrogen, and the product precipitated as a brown-red solid. The acetonitrile was then removed by rotary evaporation, the solid was dissolved in water, and a concentrated solution of ammonium hexafluorophosphate was added to precipitate the hexafluorophosphate salt. The product was filtered off onto a medium frit and washed with water, chloroform, and ether in order to remove starting materials and side products of the reaction. [1-(2-(4'-Methyl-2,2'-bipyridin-4-yl)ethyl)-1'-methyl-4,4'-bipyridinediium]-(PF$_6$)$_2$ yield 0.15 g, 2.3 × 10^{-4} mol (23%). ^{1}H NMR (CD$_3$CN) δ: CH$_3$ 2.6; N$^+$CH$_3$ 4.4; CH$_2$ 3.6, 5.0 (both triplets); aromatic 7.5–8.5.

[Ru(2,2'-bipyridine)$_2$(4-(2-(1'-methyl-4,4'-bipyridinediium-1-yl)-ethyl)-4'-methyl-2,2'-bipyridine)](PF$_6$)$_4$·2H$_2$O (H2M) and [Ru(4,4'-dimethyl-2,2'-bipyridine)$_2$(4-(2-(1'-methyl-4,4'-bipyridinediium-1-yl)-ethyl)-4'-methyl-2,2'-bipyridine)](PF$_6$)$_4$·2H$_2$O (M2M). Ru(4,4'-dimethyl-2,2'-bipyridine)$_2$(CO$_3$)·2H$_2$O (0.2 g, 3.5 × 10^{-4} mol) and Ru-(2,2'-bipyridine)$_2$(CO$_3$)·2H$_2$O (0.2 g, 3.9 × 10^{-4} mol)[13] were stirred with a slight excess (1.5 equiv) of [1-(2-(4'-methyl-2,2'-bipyridin-4-yl)-ethyl)-1'-methyl-4,4'-bipyridinediium](PF$_6$)$_2$ in 100 mL of a 1:1 ethanol/water mixture saturated with potassium nitrate for 24 h at room temperature. Most of the solvent was then removed under reduced pressure, and acetone was added to precipitate the KNO$_3$. The acetone portion was concentrated and eluted from a silica column with 5:4:1 MeCN/H$_2$O/saturated KNO$_3$ to give two bands. The product was the dark red nonfluorescent second band. The KNO$_3$ was removed by the method used earlier. Traces of [1-methyl-4,4'-bipyridinium]NO$_3$ were removed by adding water to the nitrate salt and precipitating the product as the hexafluorophosphate, which was vacuum-filtered on a medium frit and washed with small amounts of water, chloroform, and then ether. [Ru(2,2'-bipyridine)$_2$(4-(2-(1'-methyl-4,4'-bipyridinediium-1-yl)ethyl)-4'-methyl-2,2'-bipyridine)](PF$_6$)$_4$·2H$_2$O yield 0.16 g, 1.2 × 10^{-4} mol (31%). ^{1}H NMR (CD$_3$CN) δ: CH$_3$ 2.6; CH$_3$N$^+$ 4.4; CH$_2$ 3.5, 4.8 (triplets); aromatic 7.3–9.2. Anal. Calcd (found): C, 38.81 (37.85); H, 3.17 (3.13); N, 8.02 (8.06). [Ru(4,4'-dimethyl-2,2'-bipyridine)$_2$(4-(2-

(10) Geren, L.; Hahm, S.; Durham, W.; Millett, F. *Biochemistry* **1991**, *30*, 9450.

(11) Lay, P. A.; Sargeson, A. M.; Taube, H. *Inorg. Synth.* **1986**, *24*, 292.

(12) Abruna, H. D.; Breikss, A. I.; Collum, D. B. *Inorg. Chem.* **1985**, *24*, 988.

(13) Johnson, E. C.; Sullivan, B. P.; Salmon, D. J.; Adeyemi, S. A.; Meyer, T. J. *Inorg. Chem.* **1978**, *17*, 2211.

(1′-methyl-4,4′-bipyridinediium-1-yl)ethyl)-4′-methyl-2,2′-bipyridine)](PF$_6$)$_4$·2H$_2$O yield 0.13 g, 9.2 × 10^{-5} mol (26%). ^{1}H NMR (CD$_3$CN) δ: CH$_3$ 2.6; CH$_3$N$^+$ 4.4; CH$_2$ 3.5, 4.8 (triplets); aromatic 7.2–9.7. Anal. Calcd (found): C, 39.65 (39.84); H, 3.60 (3.48); N, 7.71 (7.71).

[Ru(2,2′-bipyridine)$_2$(4-(2-(1′-(cyanomethyl)-4,4′-bipyridinediium-1-yl)ethyl)-4′-methyl-2,2′-bipyridine)](PF$_6$)$_4$·2H$_2$O (H2C) and [Ru(4,4′-dimethyl-2,2′-bipyridine)$_2$(4-(2-(1′-(cyanomethyl)-4,4′-bipyridinediium-1-yl)ethyl)-4′-methyl-2,2′-bipyridine)](PF$_6$)$_4$·2H$_2$O (M2C). These compounds were made by a method different from that used for the other ethylene-linked compounds because the 1-(cyanomethyl)-4,4′-bipyridinium ion is not stable in the presence of base. Ru(2,2′-bipyridine)$_2$Cl$_2$·2H$_2$O (0.2 g, 3.8 × 10^{-4} mol) was refluxed with a slight excess (1.5 equiv) of 4-(2-bromoethyl)-4′-methyl-2,2′-bipyridine in 20 mL of 1:1 ethanol/water for 40 min. The solvent mixture was removed under reduced pressure, and then the product was eluted as two bands from a silica column using 5:4:1 MeCN/H$_2$O/saturated KNO$_3$. The luminescent second band was [Ru(2,2′-bipyridine)$_2$(4-(2-bromoethyl)-4′-methyl-2,2′-bipyridine)](NO$_3$)$_2$; the first band was brownish-black and nonluminescent. KNO$_3$ was removed by the method described above. The [Ru(2,2′-bipyridine)$_2$(4-(2-bromoethyl)-4′-methyl-2,2′-bipyridine)](NO$_3$)$_2$ was then refluxed in 50 mL of dry acetonitrile under nitrogen for 3 days with an excess (2.5 equiv) of 4,4′-bipyridine. The acetonitrile was removed by rotary evaporation, and the product was purified by dissolving in a minimum of ethanol and precipitating with ether. This procedure was repeated a few times until the decanted ether contained no 4,4′-bipyridine. Elution from silica gel using 5:4:1 MeCN/H$_2$O/saturated KNO$_3$ gave two bands. [Ru(2,2′-bipyridine)$_2$(4-(2-(4,4′-bipyridinium-1-yl)ethyl)-4′-methyl-2,2′-bipyridine)](NO$_3$)$_3$ was the second band, which was faintly luminescent. KNO$_3$ was precipitated and removed as before. [Ru(2,2′-bipyridine)$_2$(4-(2-(4,4′-bipyridinium-1-yl)ethyl)-4′-methyl-2,2′-bipyridine)](NO$_3$)$_3$ was refluxed with a 3-fold excess of bromoacetonitrile in 20 mL of MeCN under nitrogen for 8 h, and the solvent was removed by rotary evaporation. Chromatography on silica with 5:4:1 MeCN/H$_2$O/saturated KNO$_3$ gave two bands. [Ru(2,2′-bipyridine)$_2$(4-(2-(1′-(cyanomethyl)-4,4′-bipyridinediium-1-yl)ethyl)-4′-methyl-2,2′-bipyridine)](NO$_3$)$_4$ was the second band, which was nonluminescent. KNO$_3$ was removed as before, and the nitrate salt was dissolved in water and precipitated with NH$_4^+$-PF$_6^-$. The solid was separated by filtration and washed with water and ether. [Ru(4,4′-dimethyl-2,2′-bipyridine)$_2$Cl$_2$·2H$_2$O (0.2 g, 3.5 × 10^{-4} mol) was reacted similarly. Ru(2,2′-bipyridine)$_2$(4-(2-(1′-(cyanomethyl)-4,4′-bipyridinediium-1-yl)ethyl)-4′-methyl-2,2′-bipyridine)](PF$_6$)$_4$·2H$_2$O: yield 0.08 g, 5.8 × 10^{-5} mol (15%); ^{1}H NMR (CD$_3$CN) CH$_3$ 2.6, CH$_2$CN 5.8, CH$_2$ 3.5, 4.9 (triplets), aromatic 7.2–9.2. Anal. Calcd (found): C, 37.99 (38.91); H, 3.05 (2.93); N, 8.86 (8.95). [Ru(4,4′-dimethyl-2,2′-bipyridine)$_2$(4-(2-(1′-(cyanomethyl)-4,4′-bipyridinediium-1-yl)ethyl)-4′-methyl-2,2′-bipyridine)](PF$_6$)$_4$·2H$_2$O yield 0.06 g, 4.2 × 10^{-5} mol (12%). ^{1}H NMR (CD$_3$CN) δ: CH$_3$ 2.6; CH$_2$CN 5.8; CH$_2$ 3.5, 4.9 (triplets); aromatic 7.2–9.7. Anal. Calcd (found): C, 39.79 (40.90); H, 3.48 (3.46); N, 8.52 (8.58).

Picosecond Transient Absorption. Transient absorption measurements were made using a system based on a synchronously pumped dual-jet dye laser and a Nd:YAG regenerative amplifier. The pump source was a Coherent Antares 76S CW mode-locked Nd:YAG laser operating at 76 MHz. The frequency-doubled (532 nm, ca. 70 ps) ouput was adjusted to ca. 1.6 W and used to pump a Coherent 700 Series dual-jet dye laser operating with Rhodamine 6G in the gain jet and DODCI in the saturable absorber jet. Output pulses were tuned to 590 nm and monitored with a Spectra Physics 409 autocorrelator, while the saturable absorber concentration was optimized. Autocorrelation traces less than 0.7 ps were obtained before amplification. The 1064 output of the Antares 76S was adjusted to ca. 1 W and input to a Quantel RGA67-10 regenerative amplifier which, after frequency doubling, produced 70-mJ pulses of ca. 100-ps duration at 532 nm with a frequency of 10 Hz. These pulses were used to pump a Quantel Model PTA-60 dye amplifier with three amplification stages, all containing Kiton Red 620 in water as the gain medium. In order to minimize pulse broadening, a 610-nm cutoff filter was placed between the first and second amplifier stages. The output from the dual-jet dye laser was fed through the dye amplifier, resulting in a final output of ca. 2-mJ, 590-nm pulses at 10 Hz. Pulse widths were determined either by point by point autocorrelation of the 590-nm output or by observing the rise of the singlet-state absorption of tin tetrakis(*N*-methylpyridinium-4-yl)porphyrin for the 295-nm frequency-doubled output. The response profile was always better than 0.8 ps fwhm.

After frequency doubling in KDP, a dichroic mirror isolated the fundamental, which traversed a delay line before being focused into a 2-cm cell containing 50:50 H$_2$O/D$_2$O. The emerging white light continuum was recollimated, passed through a polarization scrambler and a 600-nm "notch" filter (to remove residual laser light), and split with a beam splitter to provide sample and reference beams at the cell. After passing the cell, these beams were picked up by fiber optics, dispersed through an Instruments SA spectrograph, and measured with a Princeton Instruments dual diode array connected to a personal computer. The excitation pulse traversed a fixed path and was loosely foused through the cell, at the same position as, and at a small angle to, the sample probe beam. The area of the exciting beam was roughly a factor of 4 larger than that of the probe beam at the cell.

Scheme I

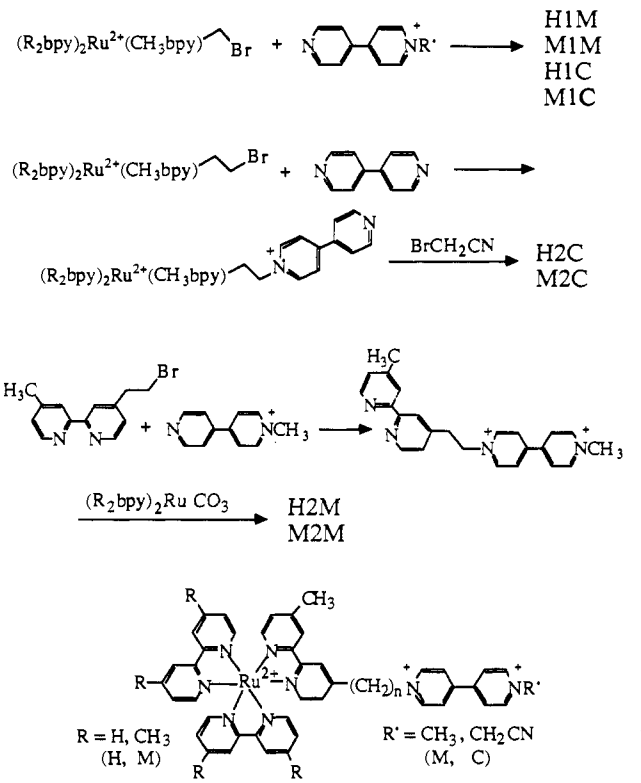

In order to make reliable measurements below 400 nm, where there is little intensity in the continuum, it was necessary to place a 370-nm band-pass filter before the fiber optics. This had the effect of preventing stray light of longer wavelength from registering on the diodes in the region of interest and allowed the use of higher probe intensities without saturating the array. The spectral chirp of the continuum was measured by observing the arrival times of stimulated Raman lines in dimethylformamide. These measurements indicated an average of 1.4 ps per 100 nm across the visible region. Since the decay lifetimes found were in the range 6–120 ps and the spectral separation of peaks used in the kinetic analysis was only 30 nm, no correction for spectral chirp was made.

Measurement of Cage-Escape Yields. Cage-escape yields for Ru(bpy)$_3^{2+}$ derivatives and viologens were measured by nanosecond flash photolysis/transient absorbance as described elsewhere.[14] Experiments were done in deoxygenated acetonitrile/0.1 M tetrabutylammonium hexafluorophosphate; the latter was recrystallized from ethanol and dried in vacuo prior to use. In all cases, the viologen concentration (10 mM) was sufficient to quench 80–92% of the luminescence, and the quenching efficiency Φ_q was determined from steady-state emission and lifetime measurements. The formation and decay of charge-separated products was monitored at the absorbance maxima of the reduced viologen monomers near 600 nm. The extinction coefficient of the methylviologen radical cation was taken from the literature.[15] For benzylviologen and (cyanomethyl)viologen, extinction coefficients (ϵ_{608} = 1.4 × 10^4, ϵ_{594} = 2.0 × 10^4, respectively) were measured spectroelectrochemically using a quartz thin-layer cell with platinum gauze electrodes. These measurements, which had an estimated accuracy of ±10%, were the largest source of error in the calculation of cage-escape yields.

Results and Discussion

Synthesis, Structure, and Electrochemistry of Linked Viologen(2+)–Ru(bpy)$_3^{2+}$ Complexes. In these studies, two different

(14) Mallouk, T. E.; Krueger, J. S.; Mayer, J. E.; Dymond, C. M. G. *Inorg. Chem.* **1989**, *28*, 3507.

(15) Watanabe, T.; Honda, K. *J. Phys. Chem.* **1982**, *86*, 2617.

Table I. Formal Potentials[a] of $Ru(bpy)_3^{2+}$–Viologen(2+) Compounds

compd	$Ru^{3+/2+}$	$V^{2+/+}$	$V^{+/0}$
H2M	+1.250	−0.400	−0.805
H2C	+1.270	−0.265	−0.665
M2M	+1.140	−0.405	−0.805
M2C	+1.135	−0.290	−0.660
H1M	+1.295	−0.360	−0.790
H1C	+1.295	−0.250	−0.590
M1M	+1.170	−0.370	−0.770
M1C	+1.180	−0.235	−0.595

[a] E_0' values were taken as the average of anodic and cathodic peak potentials vs SCE in CH_3CN/0.1 M $TBA^+BF_4^-$.

spacers, $-CH_2-$ and $-CH_2CH_2-$, were used to connect the 4′-position of the 2,2′-bipyridyl ligand with the 1-nitrogen of the viologen moiety. Scheme I summarizes the synthetic strategies used to make these compounds. The shorthand designation X*n*Y is used to describe substitution at the 4- and 4′-positions of the 2,2′-bipyridyl ligands not connected to the spacer (X = H, M), the length of the spacer (*n* = 1, 2), and substitution on the viologen nitrogen not connected to the spacer (Y = M, C). For example, H2M denotes two unsubstituted 2,2′-bipyridine ligands on Ru, a two-carbon spacer, and a methyl group on the viologen nitrogen. M1C denotes two 4,4′-dimethyl-2,2′-bipyridine ligands on Ru, a one-carbon spacer, and a cyanomethyl group on the viologen nitrogen.

Cyclic voltammetry for all eight compounds, carried out in acetonitrile/tetrabutylammonium fluoroborate, revealed the expected metal oxidation, viologen reduction, and ligand reduction waves in the range +1.6 to −1.6 V vs a saturated calomel electrode (SCE). Figure 1 shows typical plots, comparing the *n* = 1 and *n* = 2 compounds H1M and H2M. In all cases, the *n* = 1 compounds had peak potentials for all waves which were shifted to more positive values than those of their *n* = 2 relatives. This behavior can be attributed to the electron-withdrawing character of both the viologen group and the 2,2′-bipyridine ligand as felt through the one-carbon spacer. Substitution on the bipyridine ligands not attached to the spacer had very little effect on the viologen reduction potentials for both *n* = 1 and *n* = 2. Table I shows formal potentials for the ruthenium(3+/2+), viologen-(2+/1+), and viologen(1+/0) interconversions.

In order to calculate $\Delta G°$ for the forward electron-transfer reaction, it is necessary to know the excess free energy of the MLCT state. Since very rapid intramolecular electron transfer occurs in all eight compounds studied, it was not possible to determine these energies from luminescence spectra. Rather, $Ru(bpy)_2[(CH_3)_2bpy]^{2+}$ and $Ru[(CH_3)_2bpy]_3^{2+}$ were used as models for the H*n*Y and M*n*Y compounds, respectively. Their emission maxima in acetonitrile were measured, and slight shifts (+8 nm for $Ru(bpy)_2[(CH_3)_2bpy]^{2+}$ and +11 nm for $Ru[(CH_3)_2bpy]_3^{2+}$) relative to $Ru(bpy)_3^{2+}$ ($E_{0,0}$ = 2.10 eV[8]) were used to estimate MLCT energies of 2.08 and 2.07 eV, respectively.

The calculation of $\Delta G°$ also requires a correction for the thermodynamic work term, i.e., the change in donor–acceptor electrostatic interaction energy which accompanies electron transfer. This term can be approximated by pairwise summation of atomic charges according to eq 1. The summation is carried

$$\Delta G°_w \approx \Delta \sum_{ij} \frac{Z_i Z_j}{\epsilon_0 r_{ij}} \qquad (1)$$

out over all atoms *i* on the donor and *j* on the acceptor parts of the molecule. Z_i and Z_j represent the charges on the atoms, r_{ij} represents the distance between them, and ϵ_0 represents the static dielectric constant. Rather than attempt to assign fractional charges to all the atoms, we approximated $\Delta G°_w$ by placing the viologen (+1 or +2) and $Ru(bpy)_3$ (3+ or 2+) charges at their centers of mass. From CPK models, center-to-center distances were 9.2 Å for *n* = 1 and 10.4 Å for *n* = 2, assuming an extended conformation for the latter. Taking the dielectric constant as that of the solvent (ϵ_0 = 36.2) gave work terms of ±0.038 eV (*n* = 2, (−) for the forward and (+) for the back reaction) and ±0.043 eV (*n* = 1). Since these work terms are small, it was considered unnecessary to attempt a more elaborate calculation.

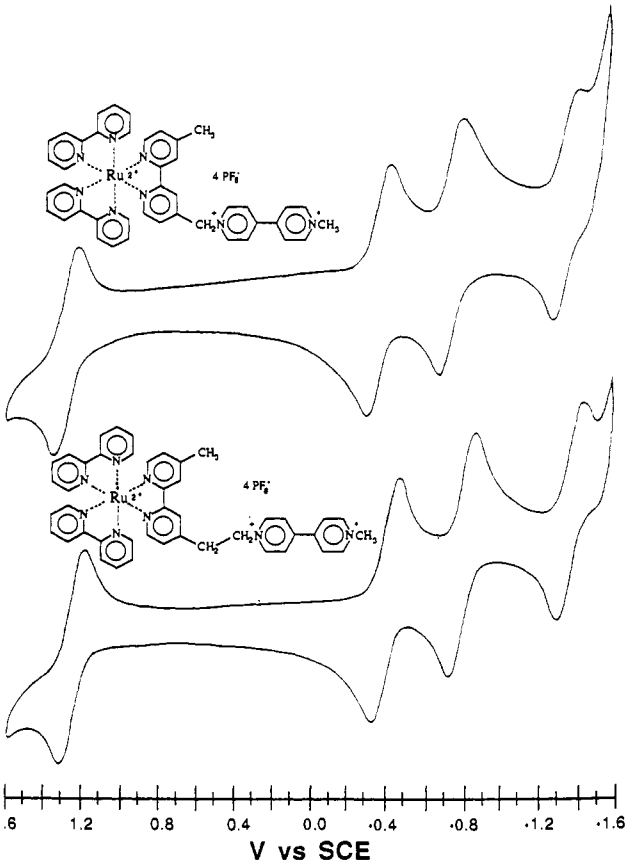

Figure 1. Cyclic voltammetry of H1M and H2M at a platinum electrode in acetonitrile/0.1 M $TBA^+BF_4^-$. Potentials are measured vs a saturated calomel electrode (SCE).

In cases where a change in free energy is required to bring the donor and acceptor parts of the molecule from their equilibrium distance to a conformation where the most rapid electron transfer occurs, a correction to the free energy of activation must also be made in Marcus plots. This extra electrostatic term can be quite significant for reactions in solvents with low dielectric constants but is less important in the present case, since our studies were carried out in acetonitrile. In the case of the *n* = 1 compounds, there is sufficiently little conformational freedom that the work term should be negligible. For the *n* = 2 compounds, we estimated this activation work term from eq 2, which was found by Cooley

$$\Delta G^{\ddagger}_w \approx \frac{Z_D Z_A}{\epsilon_0}\left(\frac{1}{r_{final}} - \frac{1}{r_{initial}}\right) \qquad (2)$$

et al.[16a] to give $\Delta G^{\ddagger}_w \leq 0.03$ eV for the forward reaction in acetonitrile (ϵ_0 = 36.2) in structurally similar $Ru(bpy)_3^{2+}$–CH_2CH_2–diquat^{2+} molecules. In this equation, r_{final} and $r_{initial}$ are respectively the donor–acceptor distance in the conformation where electron transfer occurs and the donor–acceptor distance in the equilibrium conformation (where a fully extended spacer chain was assumed). For the *n* = 2 back reactions, $\Delta G^{\ddagger}_w$ calculated from eq 2 is ≤0.02 eV.

Flash-Photolysis Experiments: Observation of the MLCT and Charge-Separated States. Figure 2 shows typical picosecond transient spectra obtained for a covalently linked $Ru(bpy)_3^{2+}$–viologen compound (M2M). The spectra are noisy at λ < 360 and λ > 500 nm, because there is very little analyzing light generated from the laser pulse at these wavelengths. However,

(16) (a) Cooley, L. F.; Larson, S. L.; Elliott, C. M.; Kelley, D. F. *J. Phys. Chem.* **1991**, *95*, 10694. (b) Larson, S. L.; Cooley, L. F.; Elliott, C. M.; Kelley, D. F. *J. Am. Chem. Soc.*, in press.

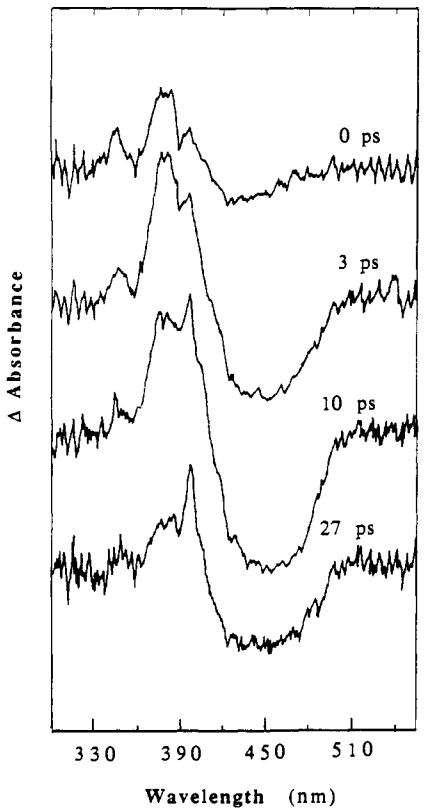

Figure 2. Transient absorbance spectra of M2M in acetonitrile, showing formation and decay of the MLCT (ca. 370 nm) and reduced viologen (ca. 400 nm) signals.

in the region between 360 and 500 nm, the signal is sufficiently strong to discern spectral features attributable to a ruthenium bipyridyl MLCT state and a reduced viologen-oxidized ruthenium charge-separated state. The former is characterized by a broad absorbance maximum at ca. 370 nm and bleaching of the ground-state absorbance at 450 nm, whereas the latter is characterized by a sharp absorbance peak at 400 nm and bleaching at 450 nm. It is evident from the spectra that the MLCT state is formed first; the "0-ps" spectrum, recorded with the 0.8-ps excitation and analyzing pulses arriving simultaneously, shows a 370-nm peak larger than the 400-nm peak. Both peaks increase with time and then decay, the MLCT state decaying more rapidly than the charge-separated state.

The rate constants for both forward and back intramolecular electron transfer may be extracted from these spectra. Since the forward electron-transfer reaction is by far the most rapid mode of decay for the MLCT state, its rate constant can be measured from a single exponential fit to the decay of the 370-nm peak. From the rise and decay of the 400-nm peak, the rate constant for the back electron-transfer reaction can also be determined. In this case, we need to consider the two-step reaction sequence (3). The rise and fall of the signal for the charge-separated state,

$$\text{MLCT} \xrightarrow{k_f} \text{Ru}^{3+}\text{-MV}^{+} \xrightarrow{k_b} \text{Ru}^{2+}\text{-MV}^{2+} \qquad (3)$$

$\text{Ru}^{3+}\text{-MV}^{+}$, are given by eq 4, in which $\Delta\epsilon_{400}$ is the change in

$$\Delta A_{400}(t) = \Delta\epsilon_{400}\left(\frac{k_f[\text{MLCT}]_0}{k_b - k_f}\right)(e^{-k_f t} - e^{-k_b t}) \qquad (4)$$

extinction coefficient for the charge-separated state relative to the MLCT and ground states and $[\text{MLCT}]_0$ is the total concentration of excited states produced initially by the flash. Since the term in large parentheses is time-independent, both rate constants can be extracted from a double-exponential fit with a single pre-exponential factor. While eq 4 contains three parameters, in practice a two-parameter fit ($[\text{MLCT}]_0$ and k_b) can be carried out, since k_f is known from the single-exponential decay

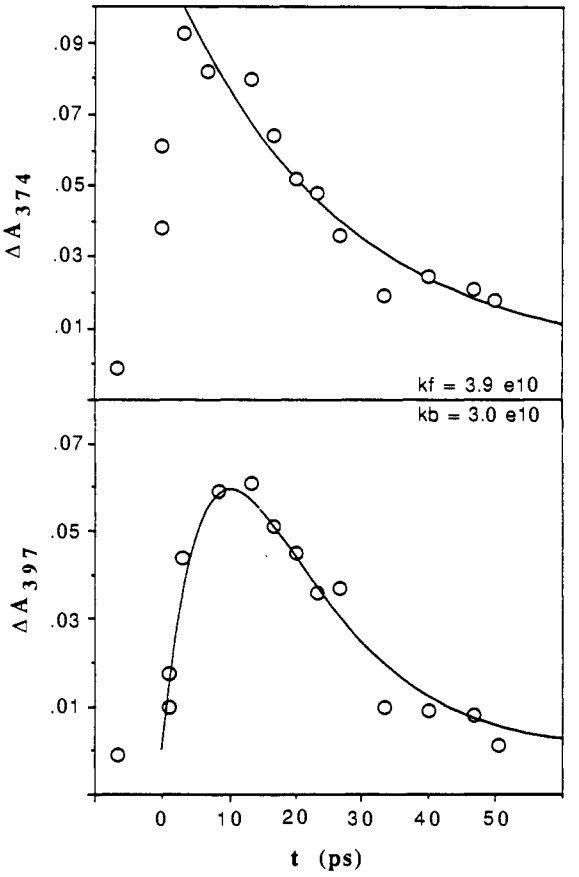

Figure 3. Transient absorbance for M2M at 374 nm (top) and 397 nm (bottom). Lines are fits to a single-exponential decay and to eq 4, respectively.

of the MLCT signal at 370 nm.

Figure 3 shows fits to a single-exponential decay, monitored at 374 nm, and a double-exponential rise and decay at 397 nm fit to eq 4 for M2M. The 397-nm data were not baseline corrected, since the MLCT state has $\Delta\epsilon \approx 0$ at this wavelength. Using this procedure, k_f and k_b could be determined for M2M and for all of the $n = 1$ compounds, although error bars were larger for k_f, $n = 1$, where $k_f > k_b$, since the 370-nm signal decayed very rapidly. For the remaining $n = 2$ compounds where the back reaction was 2–3 times faster than the forward reaction, eq 5, which is derived

$$\Delta A_{400}(t) = \Delta\epsilon_{400}\left(\frac{k_f[\text{MLCT}]_0}{k_b - k_f}\right)(e^{-k_f t}) \qquad (5)$$

from eq 4 for the case where $\exp(-k_f t) \gg \exp(-k_b t)$, was used. In this case, the 370- and 400-nm signals both decayed with the same apparent first-order rate constant, and their relative values were estimated from the ratio of the two peak heights (i.e., the pre-exponential factor in eq 5, which is time-independent).

Dependence of Forward and Back Electron-Transfer Rates on $\Delta G°$. Figure 4 shows plots of forward and back electron-transfer rate constants vs thermodynamic driving force. In all cases, the $n = 1$ compounds undergo faster electron-transfer reactions than the $n = 2$ compounds, consistent with stronger electronic coupling through the shorter saturated spacer. In general, the $n = 1$ compounds have forward rate constants larger than back rate constants, whereas the opposite is true for the $n = 2$ compounds.

The forward rate constants increase with increasing reaction exothermicity, as expected from classical Marcus theory. A similar free energy dependence was observed by Bock et al. for electron-transfer quenching of the Ru(bpy)_3^{2+} excited state by (diffusing) electron donors and acceptors,[17] and by Cooley et al.,

(17) Bock, C. R.; Connor, J. A.; Gutierrez, A. R.; Meyer, T. J.; Whitten, D. G.; Sullivan, B. P.; Nagle, J. K. *J. Am. Chem. Soc.* **1979**, *101*, 4815.

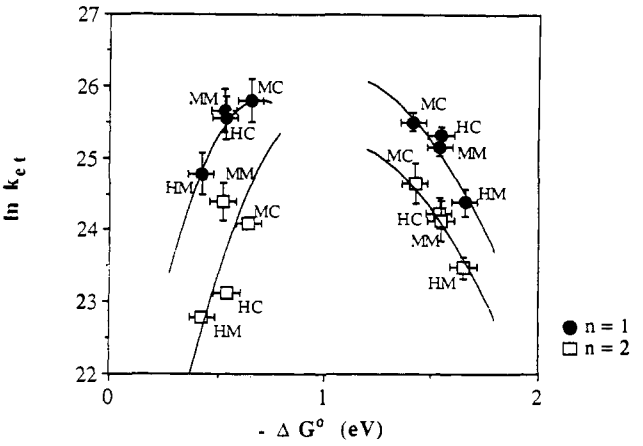

Figure 4. Plots of forward and back electron-transfer rates for $n = 1$ (filled circles) and $n = 2$ (open squares) vs thermodynamic driving force. For forward reactions, lines represent fits to eq 6 with $\lambda = 1.0$ eV, $|V(r)|^2 = 2.1 \times 10^{-3}$ eV^2 ($n = 2$), and $\lambda = 0.70$ eV, $|V(r)|^2 = 2.0 \times 10^{-3}$ eV^2 ($n = 1$). For back reactions, lines are fits to eq 7 with $h\nu = 1100$ cm^{-1}, $S = 3.0$, and $\lambda_S = 0.70$ eV. $|V(r)|^2 = 3.6 \times 10^{-4}$ eV^2 ($n = 1$) and 1.4×10^{-4} eV^2 ($n = 2$).

who examined a structurally very similar series of covalently linked $Ru(bpy)_3^{2+}$–diquat^{2+} molecules.[18] In the case of weakly adiabatic electron transfer in the normal regime, the rate constant is expected to vary with driving force according to eq 6,[19] where $V(r)$ is the

$$k_f = \frac{2|V(r)|^2}{h}\left(\frac{\pi^3}{\lambda k_B T}\right)^{1/2} \exp\left(\frac{-(\Delta G^\circ + \lambda)^2}{4\lambda k_B T} - \frac{\Delta G^\ddagger_w}{k_B T}\right) \quad (6)$$

donor–acceptor electronic coupling matrix element, λ is the sum of inner- and outer-sphere reorganization energies, T is absolute temperature, h is Planck's constant, and k_B is Boltzmann's constant. ΔG° is calculated from the formal potentials shown in Table I and the thermodynamic work term ΔG°_w, estimated from eq 1. The lines drawn through the forward rate data in Figure 4 are fits to eq 6. For the $n = 2$ data, a fit is obtained with a physically reasonable value of λ (1.0 eV), although there is some scatter in the data. Following the analysis of Cooley et al., we would expect the M2M and M2C points to lie above a line passing through the H2M and H2C points, because of unequal populations of electrons in the MLCT state on the ligands remote and adjacent to the viologen acceptor.[18] Such a trend is not evident in the $n = 2$ data, but the size of our data set is not sufficient to justify conclusions on this point.

Interestingly, the forward rate data for the $n = 1$ compounds cannot be fit to physically reasonable values of $V(r)$ and λ according to eq 6. The fit shown in Figure 4 corresponds to $\lambda = 0.7$ eV, but in this case, the value of the electronic coupling matrix element is unreasonably low (i.e., the same as that used to calculate the $n = 2$ line). While the value of the outer-sphere reorganization energy is expected to decrease with decreasing donor–acceptor distance,[3,20] the stronger electronic coupling between bipyridine and viologen groups would be expected to lead to a substantial increase in $V(r)$ relative to that of the $n = 2$ compounds, as it does for the back electron-transfer reactions (vide infra). Indeed, CPK models show that these groups are essentially in contact for $n = 1$ but not for $n = 2$. The forward electron-transfer reactions are only weakly adiabatic ($V(r) \approx (2\text{–}3)k_BT$), and in this case, the simple quadratic form implied in eq 6 should be a reasonable approximation. At present we do not have a good explanation for the unusual parameters derived from eq 6 for the $n = 1$ compounds.

The plots of back electron-transfer rate constants vs free energy difference shown in Figure 4 are quite interesting. Not only do the rates show an inverted dependence on driving force but even the $n = 1$ data can be fit quantitatively to semiclassical Marcus theory. In this case, the lines through the data correspond to fits to the semiclassical expression (7),[4b,21] which treats solvent vibrations classically and a single, or average, high-frequency vibrational mode of the donor–acceptor molecule quantum mechanically. In this expression, the total reorganization energy λ used in eq 6 has been replaced by the solvent reorganization energy λ_S. The energy of a vibrational quantum in the high-frequency internal mode is $h\nu$, and S is defined as $\lambda_v/h\nu$, where λ_v is the internal reorganization energy needed for electron transfer. While the single-mode model is questionable, especially in light of recent work by Doorn and Hupp[22] in which a large manifold of internal modes coupled to electron-transfer reactions has been detected, it is the simplest expression which can adequately represent the data. In Figure 4, both the $n = 1$ and $n = 2$ back electron-transfer data are fit to the same set of $h\nu$, S, and λ_S parameters, which are quite similar to those used by MacQueen and Schanze,[8b] and by Meyer et al.,[8a] to fit ligand–ligand back electron-transfer data into the $(bpy)Re^I(CO)_3L$ system.

$$k_b = \frac{2|V(r)|^2}{h}\left(\frac{\pi^3}{\lambda_S k_B T}\right)^{1/2} \sum_{w=0}^{\infty}(e^{-S}S^w/w!) \times \exp\left(\frac{-(\Delta G^\circ + \lambda_S + wh\nu)^2}{4\lambda_S k_B T} - \frac{\Delta G^\ddagger_w}{k_B T}\right) \quad (7)$$

A few points are worth noting in this system. First, the value of $|V(r)|^2$ for the forward transfer (at least for the $n = 2$ compounds, where it can be accurately measured) is more than an order of magnitude larger than it is for back transfer. This is because forward electron transfer (ligand-to-viologen) occurs through a much shorter spacer than does back transfer (viologen-to-metal). A very similar effect was found for $(bpy)Re^I(CO)_3L$ derivatives, where forward transfer is ligand-to-metal and back transfer, which occurs over a longer distance, is ligand-to-ligand.[7] Intervalence-transfer absorption spectra of the mixed-valence compound $[(NH_3)_5Ru(NC_5H_5)\text{–}CH_2\text{–}(C_5H_5N)Ru(NH_3)_5]^{5+}$ give calculated values[20d] of $|V(r)|^2$ which are slightly smaller (1.4×10^{-4} eV^2) than those we find for viologen–CH_2–bpy–metal back transfer (3.6×10^{-4} eV^2), consistent with slightly weaker electronic coupling through a spacer consisting of *two* pyridine ligands and one methylene group. Second, we note the correspondence between inverted-region back electron transfer in these $Ru(bpy)_3^{2+}$–viologen molecules, where the electron-transfer pathway is viologen-to-metal, and nonradiative excited-state decay in the $(bpy)Re^I(CO)_3L$ compounds, which is essentially a ligand-to-metal electron transfer. It is especially interesting to note that similar values of S, λ_S, and $h\nu$ were found in both systems.

A final point to note is that the reactions studied here are relatively weakly inverted and that they could be pushed deeper into the inverted region by increasing the driving force for the reaction or reducing the solvent reorganization energy. Increasing the value of $-\Delta G^\circ$ will unfortunately lower the forward electron-transfer rate as well, and the driving force for the back reaction cannot be increased beyond the excess free energy of the MLCT state, which is ca. 2.1 eV. However, reducing the solvent polarity should accelerate the forward rate while slowing down the back rate. In their work on donor–chromophore–acceptor (D–C–A) triads in which the C–A pair is $Ru(bpy)_3^{2+}$–diquat^{2+}, Danielson et al. have noted the formation of a charge-separated state (hole on D, electron on A) in dichloromethane but not in acetonitrile.[23] They initially attributed this effect to an increased

(18) Cooley, L. F.; Headford, C. E. L.; Elliott, C. M.; Kelley, D. F. *J. Am. Chem. Soc.* **1988**, *110*, 6673.
(19) (a) Sutin, N. *Prog. Inorg. Chem.* **1983**, *30*, 441. (b) Bruschwig, B.; Sutin, N. *Comments Inorg. Chem.* **1987**, *6*, 209.
(20) (a) Brunschwig, B. S.; Ehrenson, S.; Sutin, N. *J. Am. Chem. Soc.* **1984**, *106*, 6858. (b) Brunschwig, B. S.; Ehrenson, S.; Sutin, N. *J. Phys. Chem.* **1986**, *90*, 3657. (c) Isied, S. S.; Vassilian, A.; Wishart, J. F.; Creutz, C.; Schwarz, H. A.; Sutin, N. *J. Am. Chem. Soc.* **1988**, *110*, 635. (d) Creutz, C. *Prog. Inorg. Chem.* **1983**, *30*, 1.
(21) Miller, J. R.; Beitz, J. V.; Huddleston, R. K. *J. Am. Chem. Soc.* **1984**, *106*, 5057.
(22) Doorn, S. K.; Hupp, J. T. *J. Am. Chem. Soc.* **1989**, *111*, 1142.

electrostatic work term in the less polar solvent,[16a] which slowed charge recombination between $Ru(bpy)_3^{3+}$ and diquat$^+$. Recently,[16b] however, they have found that the quantum yield for charge separation in nonpolar solvents increases with increasing driving force for the charge recombination reaction, consistent with the finding presented here that back electron transfer between viologen(1+) and Ru^{3+} occurs in the inverted region.

Cage-Escape Yields in $Ru(bpy)_3^{2+}$–Viologen Donor–Acceptor Pairs. Since most experiments performed with $Ru(bpy)_3^{2+}$ and viologen electron acceptors have involved molecules which are not covalently linked, either in solution or in organized media such as polymers, micelles, bilayer membranes, clays, and zeolites, it is interesting to see if the inverted-region behavior found here will have consequences for those systems. In solution, the charge recombination reaction between $Ru(bpy)_3^{3+}$ and reduced viologens follows Rehm–Weller behavior;[24] i.e., it takes place at a diffusion-controlled rate[25] because of its large driving force. The slowest of our back reactions occurs over a ca. 10-Å distance (viologen-to-metal) at a rate of 10^{10} s^{-1}, which translates into a bimolecular rate constant well above the diffusion-controlled limit.[21]

Reactions which are faster than diffusion-controlled between electron-transfer products formed as geminate pairs can nevertheless be observed by measuring the quantum yield, Φ_{cs}, for formation of the charge-separated species.[5] In these experiments, one assumes that the rate at which the ions dissociate following charge transfer (k_{dis}) is independent of $-\Delta G°_{et}$, and k_b is then determined from eqs 8 and 9. The cage-escape yield, Φ_{ce}, is

$$\Phi_{ce} = \frac{k_{dis}}{k_b + k_{dis}} \tag{8}$$

$$\ln\left(\frac{1}{\Phi_{ce}} - 1\right) = \ln k_b - \ln k_{dis} \tag{9}$$

calculated as $\Phi_{ce} = \Phi_{cs}/\Phi_q$, where Φ_q is the efficiency of the electron-transfer-quenching reaction. Gould, Farid, et al. have used this technique to study the dependence of electron-transfer rate on reaction free energy and donor size in the inverted region.[6b-d,f]

Hoffman and co-workers recently reported a weak inverted dependence of k_b/k_{dis} on driving force in studies of cage-escape yield for Ru(II) diimine complexes in 4:1 H_2O/CH_3CN solutions.[26] In those solutions one expects that the solvent reorganization energy for electron transfer will be larger than in our experiments, which were carried out in acetonitrile. In their case, inverted-region electron transfer will only occur at higher driving force. We therefore measured Φ_{ce} by nanosecond flash photolysis for a series of substituted $Ru(bpy)_3^{2+}$ donors and viologen electron acceptors in acetonitrile, and the results are shown in Figure 5. One can see from this plot that over a range of ca. 0.6 eV in $-\Delta G°$, the points are widely scattered and that there is no clear correlation between reaction exothermicity and Φ_{ce}. A possible explanation for this behavior is that electron transfer occurs over a wide range of intermolecular distances in these donor–acceptor pairs and that the geometry of the encounter complex varies significantly with substitution on the donor and acceptor molecules. Since k_b and k_{dis} will both depend on these geometric factors, the free energy dependence of the back electron-transfer reaction is obscured. This behavior is in contrast to that found in organic donor–acceptor systems, where the geometry of the caged charge-separated product appears to be relatively invariant.[5,6]

Interestingly, we find that while there is scatter in the data, a noticeable trend is apparent, namely that the cage-escape yields for benzylviologen are significantly higher than they are for methylviologen or (cyanomethyl)viologen with a given photosensitizer. This is consistent with geometric factors, i.e., the larger size of benzylviologen decreasing the k_b/k_{dis} ratio. Increasing the donor–acceptor distance should in general reduce k_b, because of the exponential dependence of electron-transfer rate on distance.[14,25] The highest cage-escape yield, 77%, was measured for the benzylviologen–$Ru(bpy)_3^{2+}$ donor–acceptor pair.

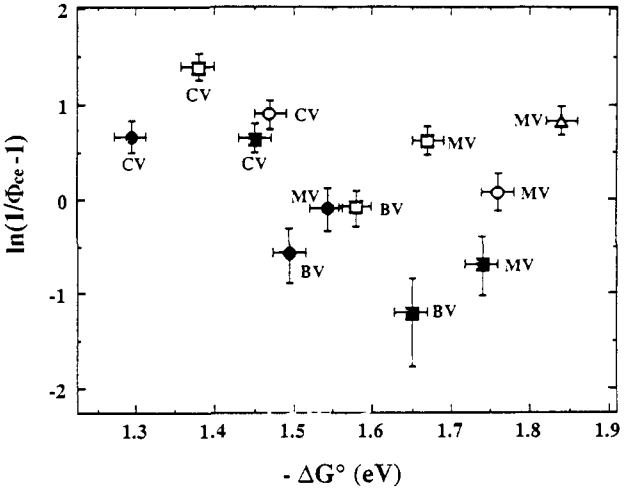

Figure 5. Plots of ln $(1/\Phi_{ce} - 1)$ vs back electron-transfer driving force for donor–acceptor pairs in acetonitrile/0.1 M $TBA^+BF_4^-$. MV, BV, and CV indicate respectively *N,N'*-dimethyl-4,4'-bipyridinediium (methylviologen), *N,N'*-dibenzyl-4,4'-bipyridinediium (benzylviologen), and *N,N'*-bis(cyanomethyl)-4,4'-bipyridinediium ((cyanomethyl)viologen) as electron acceptors. Electron donors were $Ru(bpy)_3^{2+}$ (filled squares), $Ru([CH_3]_2bpy)_3^{2+}$ (filled circles), $Ru([CH_3]_2bpy)_2(CH_3bpyCOOH)^{2+}$ (open squares), $Ru(bpy)_2(CH_3bpyCOOH)^{2+}$ (open circles), and $Ru(bpy)_2(bpy[COOH]_2)^{2+}$ (triangles). The preparation of these photosensitizers is described in ref 13.

Summary and Conclusions. Electron transfer over fixed distances in covalently linked $Ru(bpy)_3^{2+}$–viologen electron donor–acceptor molecules obeys the semiclassical Marcus relation, and both normal and inverted rate behavior are observed for the charge separation and back electron-transfer reactions, respectively. In diffusing $Ru(bpy)_3^{2+}$–viologen(2+) donor–acceptor pairs, geometric factors appear to be more important than free energy differences in determining the ratio of back reaction to geminate-pair separation rates.

These results may be of consequence for artificial photosynthetic systems in which molecules of this type are held in fixed geometries, for example in bilayer films or in solid-state media such as zeolites and clays. Since the back reaction rates are relatively weakly inverted, it is expected that the ratio of forward to back electron-transfer rates should increase as the polarity of the surrounding medium decreases. The data presented here also imply a distance dependence for the forward electron-transfer rates that is stronger than that for the back electron-transfer rates, since, for the $n = 1$ compounds, $k_f > k_b$, whereas, in the $n = 2$ compounds, $k_f < k_b$. A more detailed study of the distance dependence of intramolecular electron-transfer rates in $Ru(bpy)_3^{2+}$–viologen(2+) molecules, as well as their utilization in zeolite-based multicomponent electron-transfer chains, is currently in progress.

Acknowledgment. This work was supported by the Division of Chemical Sciences, Office of Basic Energy Sciences, Department of Energy, under Contract DE-FG05-87ER13789, and by the Welch Foundation. We thank Profs. C. M. Elliott and B. Durham for helpful pointers on synthesis and Dr. Anthony Harriman of the Center for Fast Kinetics Research, University of Texas at Austin, for assistance with spectroscopic experiments. The CFKR is supported jointly by the Biomedical Research Technology Program of the Division of Research Resources of the NIH (Grant RR00886) and by the University of Texas at Austin. T.E.M. thanks the Camille and Henry Dreyfus Foundation for support in the form of a Teacher-Scholar Award.

(23) Danielson, E.; Elliott, C. M.; Merkert, J. W.; Meyer, T. J. *J. Am. Chem. Soc.* **1987**, *109*, 2159.
(24) Rehm, D.; Weller, A. *Ber. Bunsen-Ges. Phys. Chem.* **1969**, *73*, 834.
(25) Rau, H.; Frank, R.; Greiner, G. *J. Phys. Chem.* **1986**, *90*, 2476.
(26) Ohno, T.; Yoshimura, A.; Prasad, D. R.; Hoffman, M. Z. *J. Phys. Chem.* **1991**, *95*, 4723–4728.